Fracture 1977, Volume 1, ICF4, Waterloo, Canada, June 19 - 24, 1977

PROGRESS IN THE DEVELOPMENT OF FRACTURE-MECHANISM MAPS

M. F. Ashby*

ABSTRACT

The paper describes the development of elementary fracture mechanism maps. These are maps with stress as one axis and homologous temperatures as the other, showing fields of dominance of a given micromechanism of fracture: cleavage, ductile fracture, rupture, intercrystalline creep fracture, and so on. Superimposed on the fields are contours of constant time-to-fracture, or strain-to-fracture. The maps are more difficult to make, and less reliable, than deformation-mechanism maps [1]; and one map describes only one stress state (simple tension, torsion, plane strain compression, and so on). Nevertheless, they give an overview of the micromechanisms by which a given material may fail, and help identify the one most likely to be dominant in a given experiment, or an engineering application. They should give guidance in selecting materials for high temperature use, and in the extrapolation of creep-rupture data.

INTRODUCTION

One can distinguish the fracture of a *structure* from that of a *volume element* within the structure. Here we are concerned, at least initially, with the microscopic processes which take place within a volume element as it fails. To simplify the problem, we enquire how a simple cylindrical sample, subjected to a uniform uniaxial tension (σ_1) fails. Depending on the temperature and on the material of which it is made, it may rupture by necking to zero cross-section; it may fail in a brittle manner by cleavage; it may fail by transgranular ductile fracture; or (at high temperature) by various sorts of creep fracture; some transgranular, some intergranular (Figure 1). But if one were to make a diagram with the stress σ_1 as one axis and temperature as the other, could one mark onto it with regions in which a given fracture mode is the dominant one? Wray [2] for instance, has used a schematic diagram of this general type to indicate the modes of failure of 316 stainless steel.

To do so with any precision requires some way of quantifying fracture. If, for example, we could write an expression for the strain-to-fracture or the time-to-fracture as a function of stress, σ_1, temperature, and material properties:

$$\left.\begin{aligned} \varepsilon_f &= f(\sigma_1,\ T,\ \text{Material properties}) \\ \text{or}\quad t_f &= f(\sigma_1,\ T,\ \text{Material properties}) \end{aligned}\right\} \qquad (1)$$

we could then compare these across the diagram, selecting as *dominant* the mechanism giving the smallest strain-to-fracture or time-to-fracture.

*Engineering Department, Cambridge University, Cambridge, U.K., and Division of Engineering and Applied Physics, Harvard University, Cambridge, U.S.A.

But an element is rarely subjected to such simple boundary conditions as these; the slightest necking, for instance, produces a triaxial state of stress; and at the tip of the crack, where volume elements are being successively strained-to-fracture, the stress state is again a multi-axial one. And fracture, unlike flow, does not depend on a single invariant of the stress state that we might use as an axis for the diagram. In an isotropic polycrystal, strains or times-to-fracture depend on three functions of the principal stresses. We could, then, try to express σ_f or t_f in terms of the principal stresses, or in terms of the three invariants of these. But it makes much more physical sense to take σ_1, the *maximum normal stress*, (because certain mechanisms such as boundary cavitation by void growth depend on this): τ, the *Von Mises equivalent shear stress*, (because any mechanism of fracture that requires plasticity depends on this); and p, the *hydrostatic pressure*, because the growth by plasticity of a hole depends on this and on τ.

At first sight, our diagram has now become unmanageable; three stress variables, plus the temperature, is too much to depict in any simple manner. But most of the time, we are concerned with a few straightforward stress states; uniaxial tension, equal biaxial tension, pure shear (torsion), and so on. For any one of these, the three stresses σ_1, τ, and p are proportional (Table 1) and we need take only one of them as an independent variable.

If, then, we can formulate ε_f or t_f as a function of the three stresses σ_1, τ and p, we can compute a diagram of the sort described above, with σ_n as one axis and T the other, *for a given set of boundary conditions* - uniaxial tension, for example; or torsion. If the stress state changes, the diagram will change also; but with this formulation, we should be able to compute its new form.

Our broad aim, then, is

(a) to formulate for each micromechanism of fracture, an equation of the form

$$\left.\begin{aligned} \varepsilon_f &= f(\sigma_1, \tau, p, T, \text{Material properties}) \\ \text{or} \quad t_f &= f(\sigma_1, \tau, p, T, \text{Material properties}) \end{aligned}\right\} \qquad (2)$$

(b) to evaluate these for simple tension, and compare the results with experimental data. In this way the *form* of the equation can be checked, and *unknown or arbitrary constants* in them can be matched to experimental data.

(c) to compute maps, using these adjusted equations for any given stress state.

These aims are not yet achieved; this paper summarises progress up to September, 1976.

PARALLEL BETWEEN THE CONSTRUCTION OF DEFORMATION MAPS AND OF FRACTURE MAPS

Deformation mechanism maps

The details of the approach are best explained as an adaption, to the problem of fracture, of the methods we have developed for constructing deformation-mechanism maps.

Briefly, the deformation-map method [1,3] is as follows. First, the important material properties (slip systems, moduli, diffusion coefficients, cohesive and surface energies, etc.) are critically reviewed and tabulated for the chosen material - say nickel. Then the experimental measurements of hardness, low temperature plasticity, and creep are assembled, and the equivalent shear stress τ, temperature T, shear strain-rate, $\dot{\varepsilon}$, grain size etc., of each test tabulated. This data is now plotted in one of a number of ways that allow us to assign a *mechanism of flow* to blocks of data, based on the stress exponent, the activation energy, the grain size dependence of the strain-rate, and so forth. One such data plot for nickel is shown in Figure 2.

These blocks of data are now fitted to model-based rate-equations of the form

$$\dot{\varepsilon} = \dot{\varepsilon}(\tau, T, \text{Material properties}) \qquad (3)$$

The derivation of these equations is the major theoretical part of the work. Certain mechanisms of flow (Nabarro-Herring Creep, for example) are fairly well understood, and an adequate rate equation is available in the published literature. Others - power-law creep, for instance, - are more complicated, and it becomes necessary to develop modified rate equations before data can be matched to the theory.

The method is one that combines modelling with empiricism. We develop the theory as far as possible thereby arriving at equations the *form* of which is based on physical reasoning, but which generally contain *adjustable parameters*, which are then set to give an optimum fit to the blocks of experimental data. These optimized rate equations are now used to compute deformation maps like that shown in Figure 3. A computing technique is used to evaluate the rate equations, select the dominant mechanism, plot the boundaries between fields within which a single mechanism of plasticity or creep is dominant, and add the contours of constant strain-rate. Parts of the diagram require extrapolation beyond the range of the experimental data, but the equations are based on physical models and therefore can be extrapolated with some confidence; and the method automatically replaces one mechanism by another if the second becomes dominant. A given map describes one alloy, in one state of heat treatment and grain-size; but, since grain size and other such properties are included in the rate equations, it is a trivial matter to compute a map for any given set of values for them.

We have found this approach to be practical and reasonably successful. Using it, we have produced maps for a number of common pure f.c.c., b.c.c. and h.c.p metals, three steels, and for a number of oxides, carbides and silicates. They have application in the design on interpretation of experiments, in identifying the proper constitutive law for engineering design, and in giving guidance in the extrapolation of creep data.

Fracture 1977, Volume 1

Application of the method to the construction of fracture maps

There are a number of obvious difficulties in applying this technique to fracture. First, fracture mechanisms are more complicated and less well-understood than those of plasticity and creep, so that the development of adequate equations to describe them is much more difficult. Second, fracture depends on three, not one, function of the stress state - though, (as explained in the introduction) this does not prevent us displaying the results as useful maps. Finally, (although we have considered differential formulations) the only practical form for the equations we must develop is that of equation (2). These are equations for the integral quantities ε_f or t_f, rather than the differential quantity $\dot{\varepsilon}$ of equation (3), and thus they describe an integral over the history of the sample, not an instantaneous property of it.

In spite of these difficulties, fracture-maps can be constructed: indeed, in one regard, they are easier to make than deformation maps, because the mechanisms of fracture are easier to recognize and distinguish. To illustrate the procedure, consider the problem of constructing a map for nickel.

FRACTURE MAPS FOR NICKEL DEFORMED IN UNIAXIAL TENSION

The experimental fracture map

Figure 4 shows an assembly of the fracture data for nickel which parallels the deformation data of Figure 2. The axes of the plot are *normalized tensile stress* σ_1/E (where E is Young's Modulus) and *homologous temperature* T/T_M. A point on the plot shows the stress at which nickel fractures at a given temperature; and it is labelled with the *logarithm of the time-to fracture:* $\log_{10} t_f$.

Analysis of the data allows certain boundaries between fracture mechanisms to be inserted immediately, without resorting to theory. Solid symbols indicate that the observed fracture was intercrystalline - most, though not all, investigators give sufficient metallographic information to establish this. There is no doubt that, a little above 0.6 T_m, intergranular fracture is suppressed, and *rupture* (necking to a point or chisel edge) becomes dominant. At low temperatures, fracture is by necking, followed by internal void growth and coalescence leading to a *transgranular, cup and cone, or ductile fracture.* Between this and the intergranular fracture field is a field of *transgranular creep fracture:* the material deforms by power-law creep, but fails in a way that resembles that observed during low temperature (rate-independent) plasticity.

Other materials show extra fields. Ceramics, b.c.c. and h.c.p. metals exhibit a field of *fracture by cleavage*; other materials show a regime of brittle intergranular fracture, both appearing at low temperatures. In addition, there are metallographic indications of changes of mechanism within the intergranular creep-fracture field, and perhaps within the transgranular creep-fracture field. It is important to identify and characterize these mechanisms and sub-divisions of mechanisms - each of which will appear as a field on the diagram - because they define limits for the safe extrapolation of creep rupture data: a change of mechanism invalidates all empirical extrapolation procedures.

The Construction of a Model-Based Fracture Map

The next step is to attempt to model each mechanism, deriving equations of the form of equation (2). At this stage the models are obviously over-simplified, but they combine to give a map which, in its broad aspects, matches the experimental one. The comparison reveals the deficiencies in our present physical models for the fracture process and gives guidance in improving them.

(a) *Cleavage*

Although it does not appear on a map for nickel, we include cleavage in the discussion of fracture mechanisms. Brittle solids, will, in general contain incipient cracks: let their length be $2a_o$. In more ductile solids cracks may nucleate by slip - in many instances, the crack thus nucleated has a length which scales as the grain size, d. These cracks will propagate by cleavage if the normal stress acting across the crack surface exceeds (modified) Griffith's strength, which we shall write as

$$\sigma_f = \sqrt{\frac{EG_c}{\pi a}}$$

where E is Young's modulus, G_c the energy absorbed per unit are of crack advance (its minimum value is $2\gamma_s$, where γ_s is the surface energy) and a is the crack length. The equation for cleavage then takes the form

$$\left.\begin{aligned} a &= a_o \text{ if } \tau < \tau_y \\ a &= d/2 \text{ if } \tau \geq \tau_y \end{aligned}\right\} \qquad (4a)$$

$$\left.\begin{aligned} t_f &= \infty \text{ if } \sigma_1 < \sigma_f \\ t_f &= 0 \text{ if } \sigma_1 \geq \sigma_f \end{aligned}\right\} \qquad (4b)$$

Here τ_y is the yield strength, in shear, of the material. The treatment can be extended to describe multiaxial stresses by adapting the results of McClintock and Argon [4].

(b) *Ductile Fracture at Low Temperature*

At low temperatures, plasticity is almost rate-independent. In this regime the material, if it does not cleave, fails because holes nucleate at inclusions; further plasticity makes them grow, and, when they are large enough or when the specimen itself becomes mechanically unstable, they coalesce.

A hard inclusion disturbs both the elastic and the plastic displacement field in a deformed body. The disturbance concentrates stress at the inclusion, this stress building up as the plastic strain increases [5,6,7], until the inclusion parts from the matrix or fractures. The modelling of this process, allowing for the effect of temperature, is described elsewhere [8]. The result, at low temperature, is that a fixed strain ε_i is required to nucleate holes. The strain depends on the strength of the inclusion/matrix interface and on the work hardening properties of the matrix. It can be as small as zero (for poorly wetted inclusions) and as large as 1 (for some carbides in steels); typically, it is about 0.2.

Having nucleated in this way, the holes grow until they coalesce to give a fracture path. Brown and Embury [9], building on a large body of earlier work, demonstrate that a simple geometric condition - that the holes grow until their length equals their spacing - leads to a good description* of the experimental observations. Their result is that the strain to coalescence, ε_g, is

$$\varepsilon_g = \ln\left(\frac{1}{f^{1/2}}\right)$$

where f is the volume fraction of inclusions. The strain to failure is then

$$\left.\begin{aligned} \varepsilon_f &= \varepsilon_i + \varepsilon_g \\ \text{and the time to failure is} \quad t_f &= \varepsilon_f/\dot{\varepsilon} \end{aligned}\right\} \qquad (5)$$

where $\dot{\varepsilon}$ is the strain rate.

The result can be generalized to cope with the effects of multiaxial stress stresses [4 (p.526), 10,11].

(c) *Transgranular Creep Fracture*

A material deforming by power-law creep, too, can fail by the plastic growth of holes to coalescence. If the creep rate is $\dot{\varepsilon}$, then the time to failure is again given by equation (5). A low strain-rate exponent can increase the strain to failure, ε_g, in a way that can be allowed for approximately [8].

(d) *Intergranular Creep Fracture*

At high temperatures most polycrystalline materials can fail by the nucleation of holes on grain boundaries, which grow by boundary diffusion and general plasticity (accellerated, under the right circumstances, by grain boundary sliding). The nucleation of these holes [12] and their subsequent growth [12,13,14] have been modelled in detail, though it is clear the models are still incomplete. At the simplest level, neglecting the contribution of sliding to growth, the time to fracture is given by

$$t_f = t_i + \frac{C\ kT}{\delta Z\ D_B\ \Omega\ N_B^{3/2}\sigma_1} \qquad (6)$$

and where t_i is the nucleation time, still poorly understood; C is a constant, k is Boltzmann's constant, $\delta Z\ D_B$ is the boundary thickness times its diffusion coefficient, T is the absolute temperature, Ω the atomic volume and N_B the area-density of inclusions on grain boundaries.

From a theoretical point of view, at least one other mode of intergranular fracture appears possible. If boundaries slide, as they do during power-law creep at high temperatures, holes can nucleate and grow on inclusions contained in them. The recent results of Crossman and Ashby [15] give a quantitative measure of the extent of this sliding. Their result can be

*This agreement is unexpected in that the Brown-Embury treatment does not consider specimen stability or flow-localization.

used to calculate a time-to-fracture by hole growth in boundaries, which includes both the effect of sliding and of general creep plasticity:

$$t_f = \frac{1}{\dot{\varepsilon}(df_c + (1 - f_c)r_b)} \sqrt{\frac{1}{N_B}} \qquad (7)$$

where r_b is the radius of particles, d the grain size, and f_c the "Crossman factor" which measures the extent of sliding, and itself depends on strain-rates [15].

(e) *Rupture*

If no other fracture mechanism intervenes, the sample, if pulled in a tensile mode, will neck to a point or chisel edge - that is, it will rupture. The resulting strain (or time) to fracture depends on the work-hardening, and the strain-rate sensitivity of the material, as well as on the mode of loading [15]. For uniaxial tension I have made the assumption that if no other mechanism leads to failure at a true local strain of 5 or less, then rupture intervenes. This condition is sometimes satisfied at low temperatures if the material is plastic and extremely pure, because the volume fraction of inclusions, f, is so low that the growth strain of equation (5) exceeds 5. And it is sometimes satisfied at high temperatures, even when the material is dirty, because the nucleation strain of equation (5), which increases with temperature exceeds 5.

The computed fracture map

Equations (4) to (7) have been evaluated numerically, and used to calculate a theoretical fracture map for nickel, shown in Figure 5. It is the parallel, for fracture, of the deformation map of Figure 3. In constructing it, I have used material data for nickel [2] and plausible values for the volume fractions and sizes of inclusion, and grain size, but I have made no attempt to match the equations to the observed fracture behaviour. The Figure is merely meant to illustrate that current models for the individual fracture processes, developed into equations of the type outlined above, and inserted into an appropriate computing scheme which chooses as dominant the mechanism giving the shortest time-to-fracture, leads to a map which broadly resembles the experimental one (Figure 4). The main discrepancy is the field of RUPTURE which appears on the experimental map, but not on the model-based one, because - at present - we have no good model for the effect of recrystallisation on fracture processes.

POTENTIAL USE AND EXTENSION OF THE METHOD

Extrapolation of creep-rupture data

A major problem when designing against creep fracture under steady stress and temperature, is that of extrapolating data. Many structures - nuclear reactors for instance - are designed to last for 30 years - that is, about 250,000 hours. The engineer must base his design on the extrapolation of data most of which has been obtained in 10,000 hours or less. The risk is that in this long extrapolation, new mechanisms of fracture may intervene; and as the diagrams shown here illustrate, it is impossible to extrapolate data from one field into another. Even if no new mechanisms appear, the empirical formulae used for the extrapolation may be in error; a model-based approach should lead to a better one. Finally, most fracture data is obtained in uniaxial tension; the approach is potentially able to use this data to show, not only how the fracture strain changes under some other stress state, but also whether a new mechanism appears.

Qualitative insight into fracture under non-steady stresses and temperatures

The approach, as outlined here, does not include transient behaviour and cannot give a precise description of fracture under non-steady conditions. But it may give qualitative insight into this very complicated problem. A stress cycle which carries the material from one field of the map into another introduces a new sort of damage - that characteristic of the new field. Since fracture will depend on the rates at which two (or more) sorts of damage accumulate, and on their interaction, a simple accumulation law is unlikely to work. Stress cycling within one field, on the other hand, introduces only one sort of damage, so that a simple accumulation lay may then be adequate. The same applies to temperature cycling: cycling within one field is likely to be easier to understand than cycling across a field boundary.

The development of fracture toughness maps

Finally, there is some hope that the approach might be extended to predict a way in which fracture toughness varies with stress and temperature. The fracture toughness of a material depends in a complicated way on the micromechanisms of plasticity and fracture occuring at the crack tip. As a first step in producing a diagram which illustrates how fracture toughness might vary with stress and temperature, one must assemble information on how plasticity, and the michromechanism of fracture, change with these variables, in the way outlined here.

ACKNOWLEDGEMENTS

I wish to acknowledge important discussions, criticisms and comments by R.J. Fields, C. Gandhi, Dr. H.J. Frost, Professor R. Raj, Professor J.W. Hutchinson and Dr. L.M. Brown, and the financial support of the Science Research Council of Great Britain. The work was carried out in the Engineering Department, Cambridge University, and the Division of Engineering and Applied Physics, Harvard University. C. Gandi assembled and plotted the data of Figure 4.

REFERENCES

1. ASHBY, M.F., Acat. Met., 20, 1972, 887.
2. WRAY, P.J., J. Appl. Phys., 40, 1969, 4018.
3. FROST, H.J. and ASHBY, M.F., Cambridge University Engineering Department Report "Deformation Maps for Pure Iron and Three Steels", 1975.
4. McCLINTOCK, F.A. and ARGON, A., Mechanical Behaviour of Materials, Addison-Wesley, 1966.
5. BROWN, L.M. and STOBBS, W.M., Phil. Mag. 23, 1971, 1201; to appear in Phil. Mag.,1976.
6. ARGON, A., IM, J. and SAFOGLU, R., Met. Trans. 6A, 1975, 825.
7. ARGON, A. and IM, J., Met. Trans., 6A, 1975, 839.
8. ASHBY, M.F., to appear in Acta. Met.
9. BROWN, L.M. and EMBURY, J.D., Proc. 3rd Int. Conf. on the Strength of Metals and Alloys, Institute of Metals, London, 1973.
10. RICE, J.R. and TRACEY, D.M., J. Mech. Phys. Solids, 17, 1969, 201.
11. BROWN, L.M., Churchill Conference on Fracture, Inst. of Physics, 1975.

12. RAJ, R. and ASHBY, M.F., Acta. Met 23, 1975, 653.
13. HULL, D. and RIMMER, D.E., Phil. Mag. 4, 1959, 673.
14. SPEIGHT, M.V. and HARRIS, J.E., Met. Sci. J. 1, 1967, 83.
15. CROSSMAN, F.W. and ASHBY, M.F., Acta. Met. 23, 1975, 425.

TABLE 1

(Using Von Mises equivalent stress)

STRESS STATE	σ_1	τ	p
Uniaxial Tension	1	$1/\sqrt{3}$	-1/3
Equal Biaxial Tension	1	$1/\sqrt{3}$	-2/3
Pure shear (torsion)	1	1	0
Fully constrained plane strain crack	1	$\frac{1}{2+\pi}$	$\frac{1+\pi}{2+\pi}$
Uniaxial Compression	0	$1/\sqrt{3}$	$\frac{1}{3}$
Plane strain Compression	0	$\frac{1}{2}$	$\frac{2}{3}$
Shear with pressure	$-p+\sigma$	σ	p

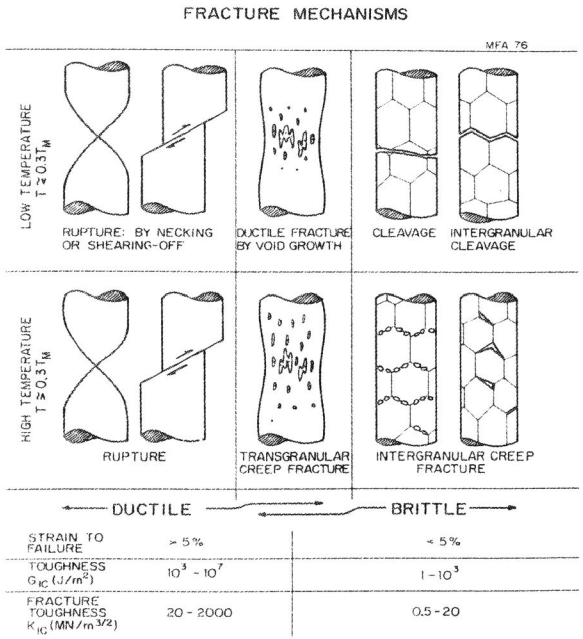

Figure 1 The mechanisms by which a cylindrical tensile specimen may fail. The upper part of the diagram refers to low temperatures, when the sample behaves as a rate-independent plastic solid. The lower part refers to processes related to those shown here, occur at the crack tip, though they are modified by the more complex state of stress there. The corresponding values of fracture toughness and toughness are given, very roughly, at the bottom on the figure.

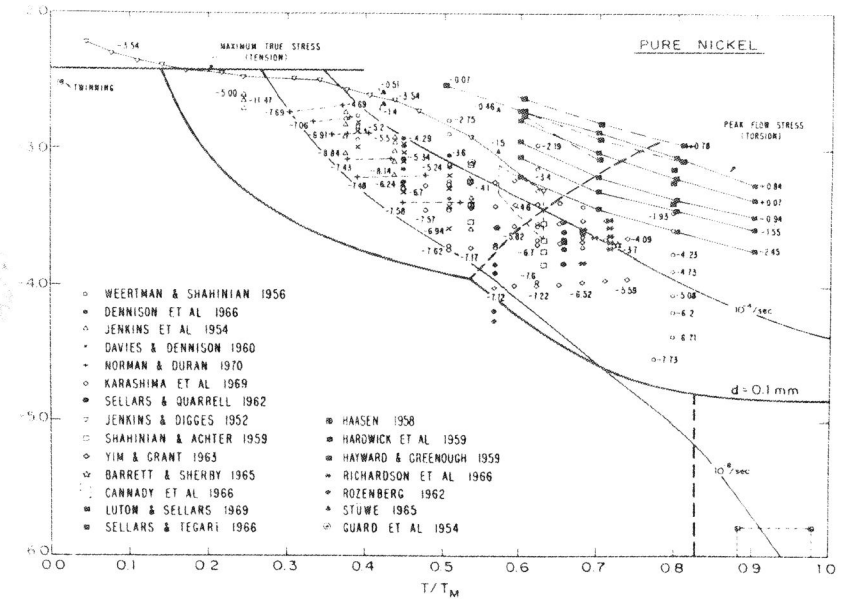

Figure 2 Plasticity and creep data for pure polycrystalline nickel. Each point describes the stress and temperature of one test, and is labelled with the logarithm, to the base 10, of the strain rate (in units of sec^{-1}). By plotting the data in this way it can be divided into blocks, and each block used to characterize one mechanism of flow. In this way the constants in the theoretical rate-equations can be determined.

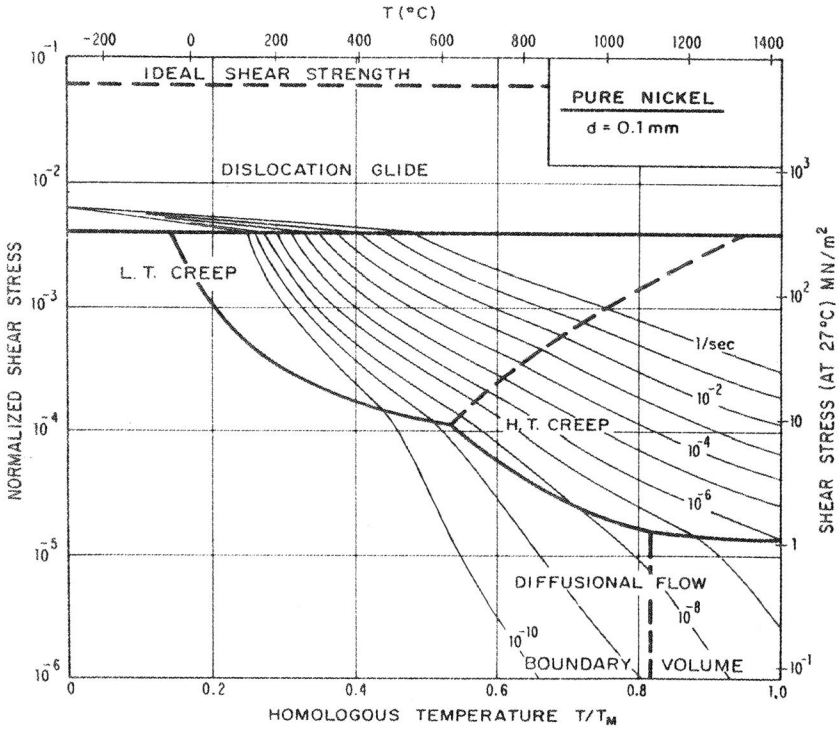

Figure 3 A deformation-mechanism map based on theoretical rate equations, but with constants, exponents, activation energies and so forth, adjusted to describe the data of Figure 2. The figure shows fields within which a given mechanism of plastic flow is dominant, and, superimposed on these, contours of constant strain rate.

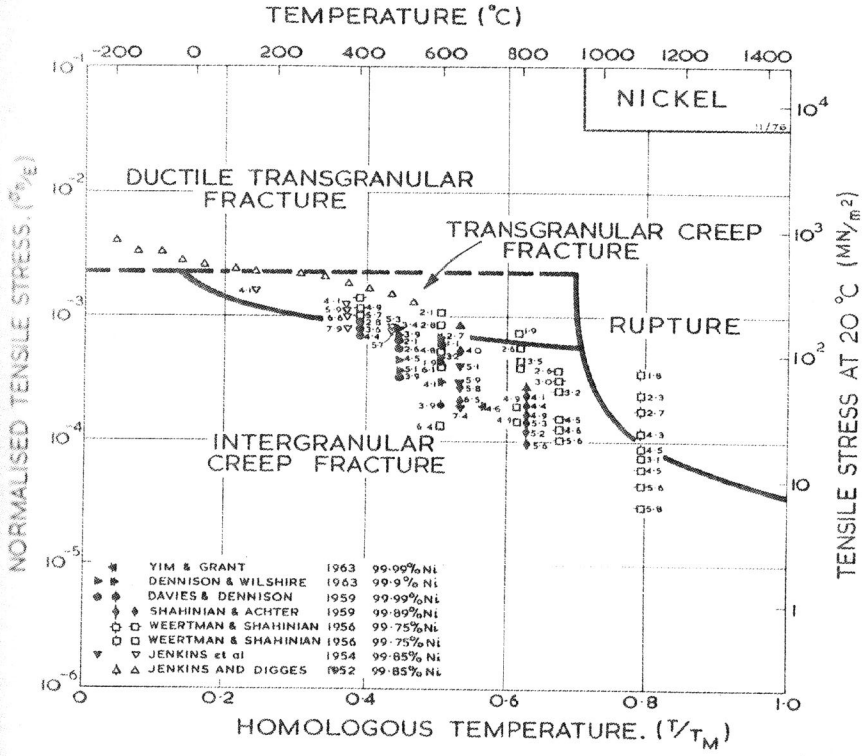

Figure 4 Fracture data for cylindrical samples of polycrystalline nickel, pulled in tension. Each point described the stress and temperature of a test and is labelled with the logarithm, to the base 10, of the time to failure (in secs). Observations of the fracture surface all the data to be divided into four blocks or fields: one for low-temperature ductile fracture, one for transgranular creep fracture, one for intergranular creep fracture and one, at high temperature, or rupture (necking to zero cross-section). Body centered cubic metals, and ceramics, show a field in which cleavage is dominant. In all materials, sub-fields exist in which variants of the basic mechanisms can be distinguished.

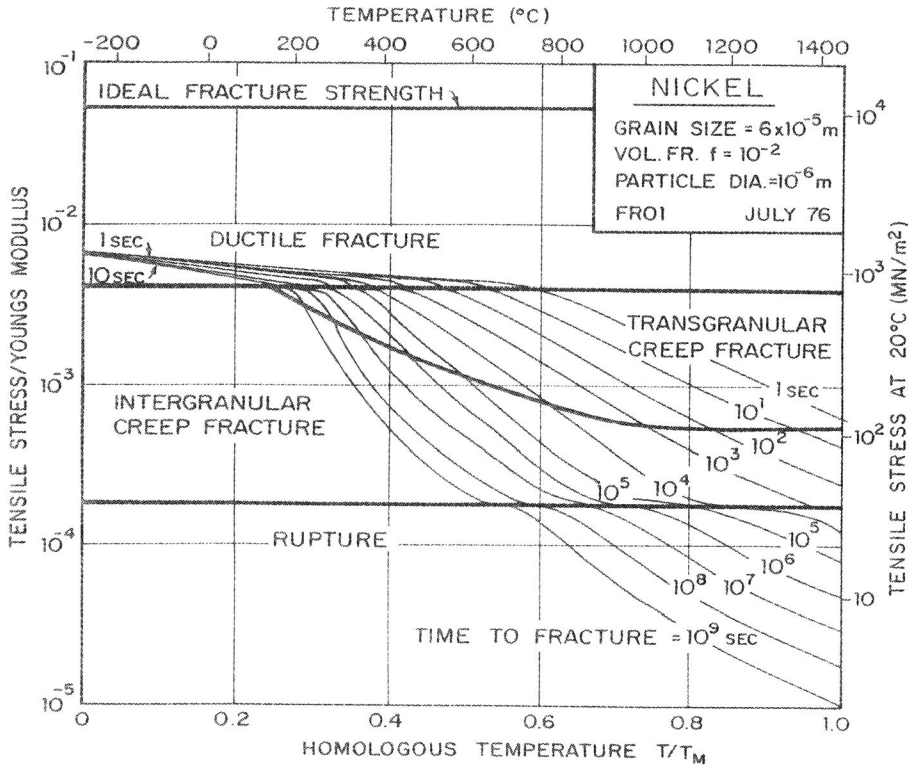

Figure 5 A computed fracture map for nickel, based on the equations outlined in the text. The figure shows the fields within which a given mechanism of fracture is dominant, and superimposed on these, contours of constant time-to-fracture.